

# Multi-Vehicle Conflict Management With Status and Intent Sharing Under Time Delays

Hao M. Wang , Sergei S. Avedisov , *Member, IEEE*, Onur Altintas, *Member, IEEE*,  
and Gábor Orosz , *Senior Member, IEEE*

**Abstract**—This paper discusses conflict analysis for multiple vehicles possessing different automation levels. Two different classes of cooperation, enabled by vehicle-to-everything (V2X) communication, are considered: status-sharing and intent-sharing. Status sharing allows vehicles to exchange their instantaneous states with each other (e.g., current velocity and position), whereas intent sharing also enables information exchange regarding the future motion of vehicles (e.g., velocity and acceleration bounds). We consider two types of time delays, one in vehicle dynamics and the other in V2X communication. Using reachability theory, our conflict analysis framework interprets the information encoded in the wireless messages pertaining to the two different cooperation classes by means of conflict charts. These charts allow for efficient and reliable on-board decision making and control design for a connected automated ego vehicle which interacts with multiple connected remote vehicles when carrying out different maneuvers. We quantify the effects of time delays in a mixed-autonomy traffic environment and unveil the benefits of intent information. Utilizing real highway data, we use numerical simulations to validate the extended conflict management framework.

**Index Terms**—Conflict analysis, connected and automated vehicles, V2X communication.

## I. INTRODUCTION

COOPERATIVE maneuvering of traffic participants may involve conflicts when their spatio-temporal paths become adequately close. Without timely detection and appropriate management, a conflict may danger the safety of individual vehicles and compromise the traffic flow efficiency. Envisioning a fully automated environment, earlier results show that vehicle-to-everything (V2X) communication can facilitate a cooperative conflict management, where vehicles seek agreements on their

future trajectories via maneuver coordination messages [1], [2], [3]. Various control techniques can then be applied to realize such cooperative maneuvers, such as optimal control [4], [5], [6], virtual platooning [7], and reachability analysis [8], [9], [10].

On the other hand, it is becoming clear that the forthcoming decades will witness an evolution dominated by the so-called mixed traffic environment, in which agents with different automation degrees and cooperation capabilities coexist [11], [12]. Recent studies started to put increasing attention on conflict resolution in such scenarios. In [13] safe maneuver of the ego vehicle is realized by computing a library of the so-called robust controlled invariant sets offline, while online estimating other vehicles' driving intentions by solving a linear programming problem. In [14] a reachable set-based trajectory prediction of road participants is proposed for provably safe motion planning, where the ego vehicle relies on on-board sensors without V2X communication, and the uncertainties of the future evolution of the environment are considered. Other methods such as game theory [15], model predictive control [16], and reinforcement learning [17] were also used for decision making and action planning of automated vehicles when interacting with human-controlled agents, especially in scenarios such as lane changes, roundabouts, and merges. However, many of these works suffer from limited scalability and heavy computational load due to the curse of dimensionality.

Focusing on a mixed autonomy environment, a framework named as conflict analysis was established in our prior works [18], [19], [20] for conflict resolution between two vehicles. The analysis was scaled up to accommodate more than two vehicles in [21]. In these studies, V2X-enabled status sharing and intent sharing were considered as means to prevent conflict. In status-sharing cooperation a connected vehicle can transmit its current measured state (e.g., GPS position and velocity). Standardized examples of status-sharing communication include Basic Safety Messages (BSMs) [22] and Cooperative Awareness Messages (CAMs) [23]. Intent-sharing cooperation involves a connected vehicle directly sharing its future motion information, for instance, the velocity and acceleration ranges for the near future [11]. With intent information, a connected vehicle can achieve a better prediction about its future environment, which benefits its decision making capabilities. However, in these works, a perfect communication neglecting packet drops and information delays was assumed, and a simplified vehicle

Manuscript received 3 October 2022; revised 12 December 2022; accepted 16 December 2022. Date of publication 23 December 2022; date of current version 20 March 2023. This work was supported by the Toyota Motor North America R&D - InfoTech Labs, Mountain View, CA, USA. (*Corresponding author: Hao M. Wang.*)

Hao M. Wang is with the Department of Mechanical Engineering, University of Michigan, Ann Arbor, MI 48109 USA (e-mail: haowangm@umich.edu).

Sergei S. Avedisov and Onur Altintas are with the Toyota Motor North America R&D - InfoTech Labs, Mountain View, CA 94043 USA (e-mail: sergei.avedisov@toyota.com; onur@computer.org).

Gábor Orosz is with the Department of Mechanical Engineering, University of Michigan, Ann Arbor, MI 48109 USA, and also with the Department of Civil and Environmental Engineering, University of Michigan, Ann Arbor, MI 48109 USA (e-mail: orosz@umich.edu).

Color versions of one or more figures in this article are available at <https://doi.org/10.1109/TIV.2022.3231639>.

Digital Object Identifier 10.1109/TIV.2022.3231639

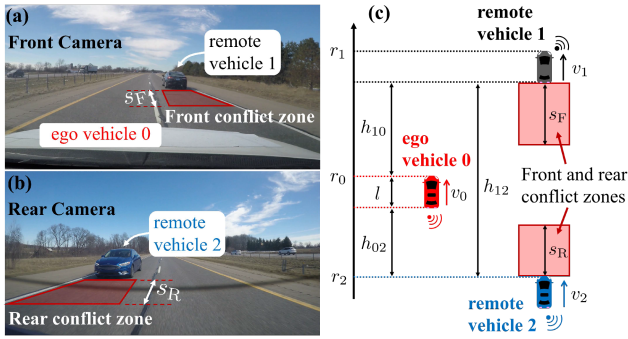


Fig. 1. Potential conflict scenario in a cooperative maneuver between three vehicles. (a)–(b) Ego vehicle 0’s view from its front and rear cameras when performing a lane change between the remote vehicles 1 and 2. (c) model showing the general scenario. Here, the front and rear conflict zones are highlighted by rectangles with red shadings.

dynamics model was used without considering computation and actuation delays.

Prior studies have shown that time delay has significant influence on the performance of connected and automated vehicles, with most research efforts focusing on vehicle platooning scenarios [24], [25], [26]. For example, time delay can contribute to the instability of vehicular chains, causing congestion and even accidents. A sizable amount of control strategies were also proposed to compensate the effects of time delay and to optimize vehicle’s performance, including predictor feedback [27] and data-based real-time optimization [28]. However, there exists a clear gap in the literature about how time delay affects conflict resolution, especially, in a mixed traffic environments in which vehicles possessing different cooperation capabilities and automation degrees interact with each other.

This study generalizes the framework of multi-vehicle conflict analysis while systematically investigating the effects of delays in both vehicle dynamics and communications, considering both status-sharing and intent-sharing cooperation. Fig. 1(a)–(b) illustrate a cooperative maneuvering scenario where conflicts may arise. Here, a connected ego vehicle attempts to change to the right lane to move between two connected remote vehicles. To perform a lane change, the following two steps are needed for the ego vehicle: (i) keep its current lane and create adequate longitudinal distances from the two remote vehicles; (ii) change its lateral position to enter the target lane. In this paper, we focus on the first step, while assuming the second step is conducted by lateral motion planning and control modules after the ego vehicle secures sufficient relative distances. We represent the safe distance buffers between the vehicles by two conflict zones attached to the remote vehicles (red rectangles in Fig. 1). To ensure a conflict-free maneuver, the ego vehicle must not overlap with either of these conflict zones before initiating the lateral move. Note that the size and shape of conflict zones can vary depending on the traffic and road conditions.

As shown in Fig. 2, we consider two types of time delays in the system. On one hand, communication delay (highlighted by green shading) is associated with generating and compiling the V2X messages on the remote vehicles, transmitting these messages, and pre-processing the received data on the ego vehicle. On the other hand, time delay in the dynamics of the

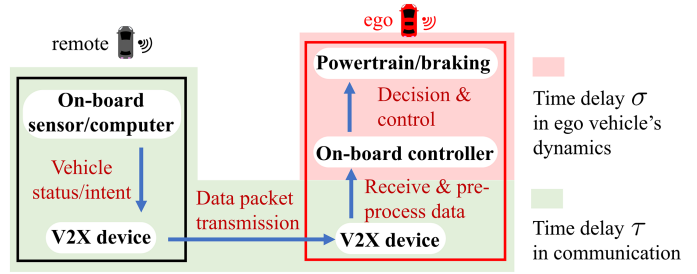


Fig. 2. Time delays in the ego vehicle’s dynamics and in the V2X communication between ego and remote vehicles.

ego vehicle (indicated by red shading) results from on-board computation time, and from the actuation time in the powertrain and braking systems.

While incorporating these time delays, this paper resolves conflicts from the ego vehicle’s viewpoint. Using reachability analysis, we propose a scalable method to calculate numerically the so-called no-conflict, uncertain, and conflict sets, which partition the state space into different domains with regard to conflict prevention. This enables fast and reliable decision making and control of the ego vehicle to guarantee conflict-free maneuvers. We study the effects of time delays on conflict prevention, and show that the information of intent substantially improves the decision and performance of the ego vehicle. Moreover, we propose a so-called goal-oriented controller to guarantee conflict-free maneuvers under time delays. This type of controller provides the designers with the freedom in choosing appropriate “goal state” to realize desired performance according to different design metrics (e.g., time and energy efficiencies, robustness). The extended framework of conflict analysis and the designed controller are demonstrated by utilizing real highway traffic data.

This paper extends our preliminary results published in the conference paper [21], compared to which, the following contributions are made in this study: (i) we generalize the multi-vehicle conflict analysis framework to accommodate time delays existing in both vehicle dynamics and V2X communication; (ii) we systematically quantify the effects of time delays on conflict in mixed autonomy environments, while revealing the benefits of intent sharing cooperation, (iii) we develop goal-oriented controller under time delays and demonstrate its applicability with real data.

The remainder of this paper is structured in the following way. In Section II, we mathematically construct the dynamic models of vehicles and provide details on the communication between vehicles. In Section III, we build conflict analysis with status sharing while investigating the effects of time delays. Conflict analysis is then extended in Section IV under intent sharing. In Section V, we design goal-oriented controller and present simulations using real traffic data. Finally, Section VI concludes the paper and lays out future research opportunities.

## II. MODELING VEHICLE DYNAMICS AND COMMUNICATION

Fig. 1(a)–(b) show the scenario we consider in this paper, where the ego vehicle 0 intends to perform a lane change between

TABLE I  
PARAMETERS VALUES USED IN THE PAPER

$s_F, s_R$	10 [m]	$l$	5 [m]
$a_{\min,0}$	-8 [m/s <sup>2</sup> ]	$a_{\min,1}, a_{\min,2}$	-4 [m/s <sup>2</sup> ]
$a_{\max,0}$	4 [m/s <sup>2</sup> ]	$a_{\max,1}, a_{\max,2}$	2 [m/s <sup>2</sup> ]
$v_{\min,0}$	22 [m/s]	$v_{\min,1}, v_{\min,2}$	25 [m/s]
$v_{\max,0}$	38 [m/s]	$v_{\max,1}, v_{\max,2}$	35 [m/s]

the remote vehicles 1 and 2. For such maneuver, as previously stated, our analysis focuses on the step (i), i.e., on vehicle 0 creating appropriate longitudinal distances before starting its lateral motion. In order to prevent conflicts, the minimum front and rear gaps represented by the lengths of conflict zones,  $s_F$  and  $s_R$ , must be secured by the ego vehicle. Here, to highlight the main idea of conflict analysis, we adopt a reasonable simplification by using  $s_F$  and  $s_R$  of constant values, as given in Table I. Such simplification is appropriate considering the limited speed domains in scenarios of normal highway driving, while the results in this paper can be extended to cases where  $s_F$  and  $s_R$  are not constant. The general model is shown in Fig. 1(c) where  $r_0, r_1$  and  $r_2$  denote the vehicles' front bumper positions, and  $v_0, v_1$  and  $v_2$  denote the vehicles' longitudinal velocities.

We describe the vehicles' longitudinal dynamics below, with the aerodynamic drag and rolling resistance neglected:

$$\begin{aligned} \dot{r}_0(t) &= v_0(t), \quad \dot{v}_0(t) = \text{sat}(u_0(t - \sigma)), \\ \dot{r}_i(t) &= v_i(t), \quad \dot{v}_i(t) = \text{sat}(u_i(t)), \quad i = 1, 2. \end{aligned} \quad (1)$$

where the dot denotes the derivative with respect to time  $t$ , and  $u_0, u_1$  and  $u_2$  are the control inputs. The limits of acceleration are modeled by the saturation function  $\text{sat}(\cdot)$ . For  $v \in (v_{\min}, v_{\max})$ , one has

$$\text{sat}(u) = \max \{ \min \{ u, a_{\max} \}, a_{\min} \}. \quad (2)$$

For  $v = v_{\min}$ , one shall substitute  $a_{\min}$  with 0, because the vehicle does not decelerate; for  $v = v_{\max}$ , one shall substitute  $a_{\max}$  with 0, since the vehicle does not accelerate. We remark that the values of acceleration and velocity limits depend on the road conditions and driving scenarios. Here we use limits corresponding to the typical driving behaviors on highways, with the assumption that the ego vehicle has the knowledge about their values; see Table I.

Note that the analysis in this paper can be carried out with different parameter values, as demonstrated in simulations in Section V. We use  $\sigma$  to denote the time delay in the ego vehicle's dynamics, which comes from its on-board computation for decision making and control, and its powertrain and braking system; see the red-shaded part in Fig. 2. Note that delays in the dynamics of remote vehicles are not explicitly included in their models, representing the ego vehicle's limited knowledge about remote vehicles' dynamics. Still, as will be shown further below, our analysis implicitly handles the potential delays in the remote vehicles' dynamics.

We consider that the vehicles can use messages pertaining to two classes of cooperation via V2X communication: status sharing and intent sharing. In case of status sharing, the remote vehicles transmit their current positions  $r_1, r_2$  and velocities  $v_1, v_2$ . When the ego vehicle receives these messages, it can use the

information for decision making and determining the control input  $u_0$ . In case of intent sharing, the remote vehicles share information about their future trajectory, such as the range of speed and acceleration in addition to their current state. This allows the ego vehicle to obtain a better prediction of the future state of the vehicles. Note that we do not have control over the remote vehicles' motions, i.e., cannot prescribe inputs  $u_1$  and  $u_2$ .

As highlighted by the green shading in Fig. 2, time delay exists in the communication between the remote and ego vehicles due to on-board sensing, and the transmission, propagation, and processing of V2X data packets. This type of delay is often referred to as communication latency. That is, the status and intent messages received by the ego vehicle contain delayed information of the remote vehicles. We use  $\tau_1$  and  $\tau_2$  to denote the communication delays of remote vehicles 1 and 2. For instance, the status messages received by the ego vehicle from the remote vehicles at a given time  $t$  contain  $r_1(t - \tau_1), v_1(t - \tau_1), r_2(t - \tau_2)$ , and  $v_2(t - \tau_2)$ . We assume that the values of  $\tau_1$  and  $\tau_2$  are known to the ego vehicle based on the GPS time stamps of the messages. Without loss of generality, we assume that the ego vehicle receives the V2X messages synchronously from both remote vehicles. The moment when the ego vehicle first receives a pair of status packets is defined as the system's initial time.

The vehicles' relative distances are defined as

$$h_{10} := r_1 - r_0 - l, \quad h_{02} := r_0 - r_2 - l, \quad h_{12} := r_1 - r_2 - l, \quad (3)$$

where  $h_{10}$  and  $h_{02}$  denote the front and rear gaps between the ego vehicle 0 and remote vehicles 1 and 2, respectively, and  $h_{12}$  denotes the total gap between the two remote vehicles; see Fig. 1(c). These gaps are signed bumper-to-bumper distances, where all three vehicles are assumed to have length  $l$ . Notice that  $h_{12} = h_{10} + h_{02} + l \geq 0$  since we assume the remote vehicle 2 to be always traveling behind vehicle 1, which yields  $h_{10} + h_{02} \geq -l$ . Because of the critical role of relative distances (3) in lane change maneuvers, the state of the system (1) is defined as

$$\mathbf{x} := [h_{10}, h_{02}, v_0, v_1, v_2]^T \in \Omega, \quad (4)$$

with the domain  $\Omega$  given by

$$\begin{aligned} \Omega := \{ & [h_{10}, h_{02}]^T \in \mathbb{R}^2 \mid h_{10} + h_{02} \geq -l \} \times [v_{\min,0}, v_{\max,0}] \\ & \times [v_{\min,1}, v_{\max,1}] \times [v_{\min,2}, v_{\max,2}]. \end{aligned} \quad (5)$$

In summary, so far we have established models for vehicle dynamics and communication. In the following sections we will carry out conflict analysis on these models.

### III. CONFLICT ANALYSIS WITH STATUS-SHARING

This section establishes conflict analysis with status-sharing. We first provide a rigorous description of conflict using formal logic. Then we develop a method based on reachability analysis to construct disjoint sets in state space with distinct qualitative behaviors in terms of conflict prevention. In addition, we study the effects of delays, appearing in the dynamics and in communication, on conflict resolution.

Recall that to prevent conflict, the ego vehicle must secure the required relative distances before changing lanes in between the two remote vehicles. Such a conflict-free condition can be formalized by the proposition

$$P := \{\exists t \geq 0, h_{10}(t) \geq s_F \wedge h_{02}(t) \geq s_R\}, \quad (6)$$

where we use the symbol  $\wedge$  (and). Proposition  $P$  can be further decomposed into three cases:

- i) No-conflict case: ego vehicle 0 is able to prevent conflict independent of the motion of remote vehicles 1 and 2.
- ii) Uncertain case: ego vehicle 0 may be able to prevent conflict depending on the motion of remote vehicles 1 and 2.
- iii) Conflict case: ego vehicle 0 is not able to prevent conflict independent of the motion of remote vehicles 1 and 2.

These cases correspond to three pairwise disjoint sets in the state space  $\Omega$  of system (1). Namely, we define

$$\mathcal{P}_g := \{\mathbf{x}(0) \in \Omega | \forall u_1(t), \forall u_2(t), \exists u_0(t), P\}, \quad (7)$$

$$\mathcal{P}_y := \{\mathbf{x}(0) \in \Omega | (\exists u_1(t), \exists u_2(t), \forall u_0(t), \neg P) \wedge (\exists u_1(t), \exists u_2(t), \exists u_0(t), P)\}, \quad (8)$$

$$\mathcal{P}_r := \{\mathbf{x}(0) \in \Omega | \forall u_1(t), \forall u_2(t), \forall u_0(t), \neg P\}, \quad (9)$$

where the symbol  $\neg$  means negation, and  $u_0(t)$ ,  $u_1(t)$ , and  $u_2(t)$  are functions of time  $t \geq 0$ . These sets are referred to as no-conflict set, uncertain set, and conflict set, respectively. The corresponding domains are visualized in the state space  $\Omega$  with green, yellow, and red colors in the remaining of the paper, and therefore, we use “g,” “y,” and “r” as subscripts. Note that the definition (8) contains two predicates which negate those of (7) and (9), i.e.,

$$(\exists u_1, \exists u_2, \forall u_0, \neg P) \iff \neg(\forall u_1, \forall u_2, \exists u_0, P), \quad (10)$$

$$(\exists u_1, \exists u_2, \exists u_0, P) \iff \neg(\forall u_1, \forall u_2, \forall u_0, \neg P). \quad (11)$$

Therefore, the sets  $\mathcal{P}_g$ ,  $\mathcal{P}_y$ , and  $\mathcal{P}_r$  are indeed pairwise disjoint, and  $\mathcal{P}_g \cup \mathcal{P}_y \cup \mathcal{P}_r = \Omega$ .

#### A. Conflict Analysis With Time Delay in Dynamics

In this subsection, we develop theorems for conflict analysis considering time delay in the ego vehicle’s dynamics while assuming zero communication delays for both remote vehicles.

Fig. 3(a) and (b) show the sets  $\mathcal{P}_g$ ,  $\mathcal{P}_y$ , and  $\mathcal{P}_r$  in  $(h_{10}, h_{02})$ -plane for delays  $\sigma = 0$  [s] and  $\sigma = 0.5$  [s] in the ego vehicle’s dynamics, respectively, while considering the velocities  $(v_0, v_1, v_2) = (27, 29, 28)$  [m/s]. The domain outside the set  $\Omega$  is left blank; cf. (5). These are referred to as conflict charts, and their derivations are discussed further below. Given the current vehicle status the conflict charts can be used to determine the possibility of conflict-free lane change in the future. Notice that for any finite delay  $\sigma$  in the ego vehicle’s dynamics, we have  $\mathcal{P}_r = \emptyset$  if the parameters of behavior limits satisfy the condition

$$(v_{\max,1} > v_{\min,2}) \wedge (v_{\max,0} > v_{\min,2}) \wedge (v_{\min,0} < v_{\max,1}), \quad (12)$$

cf. parameters in Table I. This condition enables the remote vehicles to create sufficiently large distance between them (if

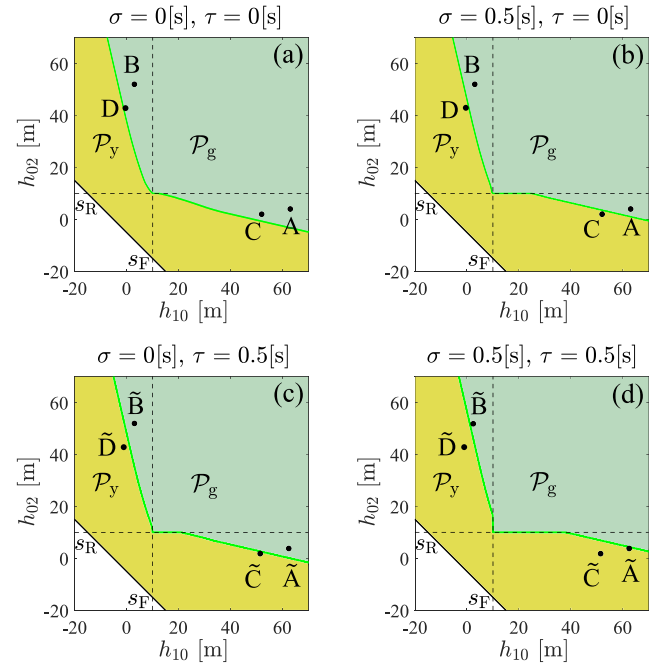


Fig. 3. Conflict charts in  $(h_{10}, h_{02})$ -plane under the indicated values of delay  $\sigma$  in the ego vehicle’s dynamics and communication delay  $\tau_1 = \tau_2 = \tau$ . (a) For velocities  $(v_0(0), v_1(0), v_2(0)) = (27, 29, 28)$  [m/s] without delays. (b) For the same velocities as (a) with delay  $\sigma$  and control input history  $u_0(t) = 0$  [m/s<sup>2</sup>],  $t \in [-\sigma, 0]$ . (c) For velocities  $(v_0(0), v_1^{\text{est}}(0), v_2^{\text{est}}(0)) = (27, 26.7, 28.85)$  [m/s] with communication delay  $\tau$ , where  $v_1^{\text{est}}(0), v_2^{\text{est}}(0)$  are estimated based on Theorem 2. (d) For the same velocities as (c) with both delays  $\sigma$  and  $\tau$ .

vehicle 1 speeds up and vehicle 2 decelerates), such that the ego vehicle can eventually perform a conflict-free lane change. Therefore, our focus will be the sets  $\mathcal{P}_g$  and  $\mathcal{P}_y$  throughout the rest of this subsection. We remark that if a maneuver needs to be completed within certain time deadline, then  $\mathcal{P}_r = \emptyset$  may no longer hold and additional investigation on  $\mathcal{P}_r$  is needed. This is left for future work.

Next we introduce a method to check whether a given initial state  $\mathbf{x}(0)$  is located in the set  $\mathcal{P}_g$  or in the set  $\mathcal{P}_y$ . One may construct these sets by examining each state in the state space  $\Omega$ , but it is not necessary to compute them on-board. Instead, once receiving the latest V2X information, the ego vehicle only needs to determine which set the current system state belongs to. At the initial time, if  $h_{10}(0) \geq s_F \wedge h_{02}(0) \geq s_R$  holds, then  $\mathbf{x}(0) \in \mathcal{P}_g$  holds immediately since the required front and rear gaps are already formed. Otherwise, it becomes necessary to examine whether the proposition  $P$  in (6) holds for some  $t > 0$ , while taking into account the ego and remote vehicles’ all possible future trajectories. The following Lemma states that the remote vehicles’ behavior limits shall be used to check  $\mathbf{x}(0) \in \mathcal{P}_g$ .

**Lemma 1:** For any given initial state  $\mathbf{x}(0) \in \Omega$ , the following relationship holds:

$$\begin{aligned} \{\forall u_1(t), \forall u_2(t), \exists u_0(t), P\} &\iff \{(u_1(t), u_2(t)) \\ &\equiv (a_{\min,1}, a_{\max,2}), \exists u_0(t), \exists t \in T, h_{10}(t) \geq s_F \wedge h_{02}(t) \geq s_R\}, \end{aligned} \quad (13)$$

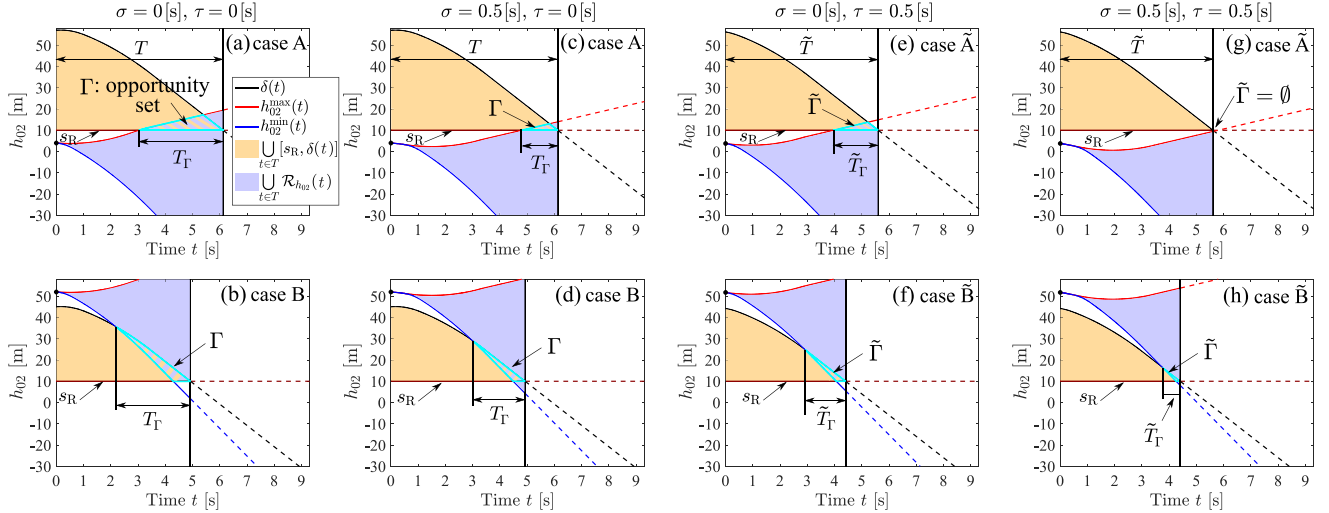


Fig. 4. Opportunity set  $\Gamma$  for the indicated values of time delays with: (a)–(d) initial states corresponding to point A  $(h_{10}(0), h_{02}(0)) = (63, 4)$  [m] and point B  $(h_{10}(0), h_{02}(0)) = (3, 52)$  [m] in Fig. 3(a)–(b); (e)–(h) estimated initial states under communication delays corresponding to point  $\tilde{A}$   $(h_{10}^{\text{est}}(0), h_{02}^{\text{est}}(0)) = (62.43, 3.79)$  [m] and point  $\tilde{B}$   $(h_{10}^{\text{est}}(0), h_{02}^{\text{est}}(0)) = (2.43, 51.79)$  [m] in Fig. 3(c)–(d).

where  $T = \{t \geq 0 | h_{12}(t) \geq s_F + s_R + l\}$ .

*Proof:* See Appendix A.  $\square$

Here,  $T$  represents the time interval during which the total gap between the two remote vehicles is large enough for the ego vehicle to form the required front and rear gaps, assuming the remote vehicles' worst-case behaviors given by their input limits. Combining (7) and (13), Lemma 1 suggests that to prevent conflict independent of remote vehicles' behaviors, the ego vehicle must form the front and rear gaps within the time interval  $T$ . Thus, checking  $\mathbf{x}(0) \in \mathcal{P}_g$  is equivalent to checking the existences of an input  $u_0(t)$  for  $t \geq 0$  and a time  $t \in T$  such that  $h_{10}(t) \geq s_F \wedge h_{02}(t) \geq s_R$  holds under the remote vehicles' worst-case behaviors. Note that with delay  $\sigma$  in the dynamics, control input assigned to the ego vehicle only “kicks in” after  $\sigma$  time. Therefore, the motion of the ego vehicle during the time interval  $[0, \sigma]$  is determined by its control input history, i.e.,  $u_0(t)$ ,  $t \in [-\sigma, 0]$ . Also notice that the consideration of remote vehicles' worst-case behaviors in Lemma 1 represents the most adversarial scenario even under the potential delays in their dynamics and the unknown control input histories. We remark that our analysis can be adapted to the case where the ego vehicle has the knowledge about the remote vehicles' delays in the dynamics and their corresponding control input histories, which will lead to less conservative results.

Now we are ready to state a theorem that allows us to determine whether conflict-free maneuvers are possible based on the behavioral limits of the ego vehicle and of the remote vehicles. More precisely, the Theorem below gives a reachability-based criterion to check  $\mathbf{x}(0) \in \mathcal{P}_g$ .

*Theorem 1:* Given the dynamics (1)–(2) and the initial state  $\mathbf{x}(0) \in \Omega$ ,  $\mathbf{x}(0) \in \mathcal{P}_g$  holds if and only if the condition

$$\Gamma := \bigcup_{t \in T} [s_R, \delta(t)] \cap \bigcup_{t \in T} \mathcal{R}_{h_{02}}(t) \neq \emptyset, \quad (14)$$

is satisfied under  $(u_1(t), u_2(t)) \equiv (a_{\min,1}, a_{\max,2})$ , where  $\delta(t) = h_{12}(t) - s_F - l$ ,  $\mathcal{R}_{h_{02}}(t) = [h_{02}^{\min}(t), h_{02}^{\max}(t)]$ , and the analytical forms of  $\delta(t)$ ,  $h_{02}^{\min}(t)$ , and  $h_{02}^{\max}(t)$  are given in Appendix B.

*Proof:* See Appendix C.  $\square$

Here the set  $\bigcup_{t \in T} [s_R, \delta(t)] \subseteq T \times \mathbb{R}$  contains the time  $t$  and the rear gap values  $h_{02}$  such that the conflict-free condition  $h_{10}(t) \geq s_F \wedge h_{02}(t) \geq s_R$  holds under the remote vehicles' worst-case behaviors, while ignoring the ego vehicle's motion capability; see the orange shaded region in Fig. 4(a). Note that  $\delta(t) \geq s_R$  defines the time interval  $T$  (cf. Lemma 1), when an adequate gap exists between the remote vehicles 1 and 2. On the other hand, the set  $\bigcup_{t \in T} \mathcal{R}_{h_{02}}(t) \subseteq T \times \mathbb{R}$  gives all rear gap values that the ego vehicle is able to reach along the time interval  $T$ , which corresponds to the projection of the (space-time) reachable tube of system (1) onto the  $(t, h_{02})$  domain; see the light purple shaded region in Fig. 4(a). Note that for any given time  $t > 0$ ,  $\mathcal{R}_{h_{02}}(t)$  can be described by a lower bound  $h_{02}^{\min}(t)$  and an upper bound  $h_{02}^{\max}(t)$ ; see the blue and red curves in Fig. 4(a). They are calculated using the input limits  $(u_0(t), u_2(t)) \equiv (a_{\min,0}, a_{\max,2})$  and  $(u_0(t), u_2(t)) \equiv (a_{\max,0}, a_{\max,2})$  on  $t > 0$ , while considering the control input history  $u_0(t)$  on  $t \in [-\sigma, 0]$ . Thus, the intersection  $\Gamma$  of sets  $\bigcup_{t \in T} [s_R, \delta(t)]$  and  $\bigcup_{t \in T} \mathcal{R}_{h_{02}}(t)$  defined in (14) gives all feasible rear gaps and the corresponding times when the ego vehicle can secure  $h_{10}(t) \geq s_F \wedge h_{02}(t) \geq s_R$  independent of the remote vehicles' behaviors; see the striped region in Fig. 4(a). Such set  $\Gamma$  is referred to as opportunity set, and the opportunity window it covers is denoted by  $T_\Gamma$ .

Note that since the ego vehicle has the knowledge of its own control input history, it is sufficient to construct the opportunity set  $\Gamma$  for the given history of  $u_0(t)$  under delay  $\sigma$ . On the other hand, to ensure that a conflict-free maneuver exists independent of the ego vehicle's control input history, the set  $\Gamma$  needs to be constructed considering all possible histories, i.e., all functions

$u_0(t)$ ,  $t \in [-\sigma, 0]$ . We remark that this is consistent with the infinite-dimensional nature of time delay systems [29], [30], but is outside the scope of this paper. We leave the corresponding analysis for future work.

It is emphasized that using Theorem 1, checking  $\mathbf{x}(0) \in \mathcal{P}_g$  is converted to examining the intersection of two analytically given sets. This is implementable in real time by applying simple yet efficient numerical algorithms. On the other hand, with more detailed vehicle dynamics, analytical form of the set  $\mathcal{R}_{h_{02}}(t)$  may no longer be available. In this case reachable sets can still be constructed using a plethora of approximation techniques [31]. The ego vehicle's decision on its maneuver can be made based on the opportunity set  $\Gamma$ . If  $\Gamma \neq \emptyset$ , i.e.,  $\mathbf{x}(0) \in \mathcal{P}_g$ , then conflict is preventable, and the ego vehicle shall decide to pursue the opportunity of changing the lane. If  $\Gamma = \emptyset$ , i.e.,  $\mathbf{x}(0) \in \mathcal{P}_y$ , then a conflict-free lane change is not guaranteed. In such a scenario the ego vehicle shall decide to stay in its current lane.

Having established the theoretical base for conflict analysis under time delay  $\sigma$ , let us now investigate the effects of  $\sigma$  on conflict resolution. Fig. 4(a)–(b) illustrate the opportunity sets corresponding to the initial states given by points A and B in the conflict chart in Fig. 3(a) without delay ( $\sigma = 0$  [s]). Note that in case A the ego vehicle is initially behind both remote vehicles, while in case B the ego vehicle is initially in front of them. For delay  $\sigma = 0.5$  [s], the opportunity sets for initial states A and B are constructed in Fig. 4(c)–(d) for the given control input history  $u_0(t) \equiv 0$  on  $t \in [-\sigma, 0]$ ; see also Fig. 3(b) for the corresponding conflict chart. In fact, as delay  $\sigma$  in the dynamics increases, the opportunity set  $\Gamma$  shrinks, independent of the given initial state and control command history. This is summarized in the following corollary.

*Corollary 1.1:* Given initial state  $\mathbf{x}(0) \in \Omega$ , let  $\Gamma$  and  $\hat{\Gamma}$ , and  $T_\Gamma$  and  $\hat{T}_\Gamma$  be the opportunity sets and their time windows under delays  $\sigma$  and  $\hat{\sigma}$  in the ego vehicle's dynamics, such that  $\sigma \leq \hat{\sigma}$ . Then, we have

$$\Gamma \supseteq \hat{\Gamma}, \quad T_\Gamma \supseteq \hat{T}_\Gamma. \quad (15)$$

Moreover, let  $\mathcal{P}_g$  and  $\hat{\mathcal{P}}_g$ , and  $\mathcal{P}_y$  and  $\hat{\mathcal{P}}_y$  be the no-conflict sets and uncertain sets corresponding to  $\sigma$  and  $\hat{\sigma}$ . Then

$$\mathcal{P}_g \supseteq \hat{\mathcal{P}}_g, \quad \mathcal{P}_y \subseteq \hat{\mathcal{P}}_y. \quad (16)$$

That is, the green no-conflict set shrinks whereas the yellow uncertain set expands as delay  $\sigma$  increases. The relationship (15) can be shown from the fact that larger delay in the dynamics leads to smaller set  $\mathcal{R}_{h_{02}}(t)$  in (14). The relationship (16) can then be derived from (15) and Theorem 1.

The heat map shown in Fig. 5(a) quantifies the decrease of the opportunity window  $\Delta T_\Gamma := |\hat{T}_\Gamma| - |T_\Gamma|$  when delay in the dynamics increases from 0 [s] to 0.5 [s]. Solid and dashed green curves correspond to the boundaries between the no-conflict and uncertain domains for  $\sigma = 0$  [s] and  $\sigma = 0.5$  [s] respectively. Here, the norm  $|\cdot|$  measures the length of one-dimensional set. The stripped region corresponds to scenarios where the no-conflict domain changed to the uncertain domain as the delay in dynamics increased; see initial states represented by points C and D. In this region the ego vehicle cannot be certain of

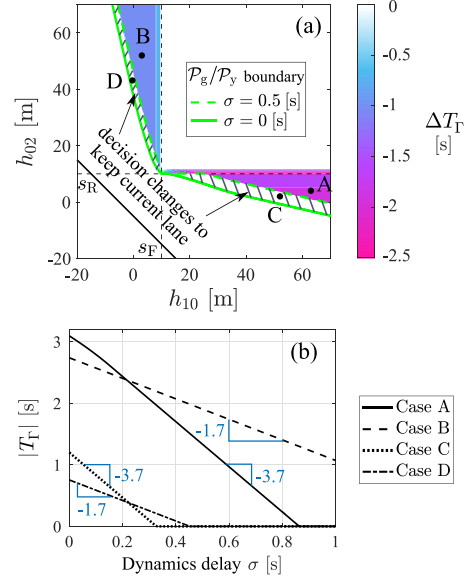


Fig. 5. (a) Heat map showing the decrease of opportunity window  $\Delta T_\Gamma = |\hat{T}_\Gamma| - |T_\Gamma|$  when delay in the ego vehicle's dynamics increases from  $\sigma = 0$  [s] to  $\sigma = 0.5$  [s]. (b) Opportunity window length evaluated as a function of delay  $\sigma$  for initial state cases represented by points A-D in Fig. 3(a)–(b), where  $(v_0(0), v_1(0), v_2(0)) = (27, 29, 28)$  [m/s], and A  $(h_{10}(0), h_{02}(0)) = (63, 4)$  [m], B  $(h_{10}(0), h_{02}(0)) = (3, 52)$  [m], C  $(h_{10}(0), h_{02}(0)) = (52, 2)$  [m], and D  $(h_{10}(0), h_{02}(0)) = (-0.5, 43)$  [m].

a conflict-free lane change any more, and thus decides not to undertake a lane change between the remote vehicles. In the region where the decision of the ego vehicle remains to change lane, the opportunity window still decreases; see the region above the dashed green boundary.

Fig. 5(b) quantifies the opportunity window length  $|T_\Gamma|$  while varying delay  $\sigma$  in the dynamics for initial states A-D. The slopes of the indicated segments on these curves being smaller than  $-1$  reveals that the increase of delay in the dynamics can result in significantly larger decrease of opportunity window for conflict-free maneuvers. This contradicts an intuitive notion that every 0.1 [s] of delay results in 0.1 [s] degradation of the opportunity window. The slope differences between cases A and B (and also between cases C and D) result from the fact that the ego vehicle was initially traveling slower than both remote vehicles. Thus, the increase of delay  $\sigma$  impacts more opportunity of changing lane from back (cases A and C) than changing lane from front (cases B and D).

To summarize, so far we have developed an efficient method for conflict analysis with time delay in vehicle dynamics via Theorem 1. This allows us to quantify the effects of this delay in terms of the degradation of opportunity window for a conflict-free lane change. The established theory provides a basis for further analysis under the communication time delays as discussed in the subsection below.

## B. Conflict Analysis With Time Delays in Communication

In this subsection, we extend conflict analysis to the case when communication delays  $\tau_1$  and  $\tau_2$  exist in the status information of the remote vehicles 1 and 2.

At the initial time, the ego vehicle has access to its own current status  $r_0(0)$ ,  $v_0(0)$ , and the remote vehicles' delayed status  $r_1(-\tau_1)$ ,  $v_1(-\tau_1)$ ,  $r_2(-\tau_2)$ , and  $v_2(-\tau_2)$ . That is, the exact initial state  $\mathbf{x}(0)$  is no longer available to the ego vehicle, and thus, checking  $\mathbf{x}(0) \in \mathcal{P}_g$  is not implementable. We remark, however, that while the communication delays compromise the ego vehicle's awareness of the exact current state, the sets  $\mathcal{P}_g$ ,  $\mathcal{P}_y$ , and  $\mathcal{P}_r$  remain the same, still representing the ground truth of conflict prevention based on state values; see definitions in (7)–(9).

Since the ego vehicle has no knowledge about the actual behaviors of the remote vehicles 1 and 2 during the past time intervals  $[-\tau_1, 0)$  and  $[-\tau_2, 0)$ , we modify the propositions corresponding to no-conflict, uncertain, and conflict cases as

$$\tilde{P}_g := \quad (17)$$

$$\{\forall u_1(t) \text{ on } t \geq -\tau_1, \forall u_2(t) \text{ on } t \geq -\tau_2, \exists u_0(t) \text{ on } t \geq 0, P\},$$

$$\tilde{P}_y := \quad (18)$$

$$\{\exists u_1(t) \text{ on } t \geq -\tau_1, \exists u_2(t) \text{ on } t \geq -\tau_2, \forall u_0(t) \text{ on } t \geq 0, \neg P\} \wedge$$

$$\{\exists u_1(t) \text{ on } t \geq -\tau_1, \exists u_2(t) \text{ on } t \geq -\tau_2, \exists u_0(t) \text{ on } t \geq 0, P\},$$

$$\tilde{P}_r :=$$

$$\{\forall u_1(t) \text{ on } t \geq -\tau_1, \forall u_2(t) \text{ on } t \geq -\tau_2, \forall u_0(t) \text{ on } t \geq 0, \neg P\}, \quad (19)$$

cf. in (7)–(9). Note that independent of the given (delayed) vehicle status, the parameter condition (12) still allows the remote vehicles to form adequately large distance to eventually enable a conflict-free lane change, which yields  $\tilde{P}_r = \text{false}$  (and thus,  $\mathcal{P}_r = \emptyset$  still holds). Therefore, we focus on propositions  $\tilde{P}_g$  and  $\tilde{P}_y$  in the rest of this subsection.

The following Theorem reveals that by appropriately estimating the current state, the methodology introduced in the previous subsection can be applied to determine if a conflict is preventable under communication delays.

*Theorem 2:* Given the dynamics (1)–(2) and vehicle status  $r_0(0)$ ,  $v_0(0)$ ,  $r_1(-\tau_1)$ ,  $v_1(-\tau_1)$ ,  $r_2(-\tau_2)$ , and  $v_2(-\tau_2)$ , the following relationships hold:

$$\tilde{P}_g \iff \mathbf{x}_{\text{est}}(0) \in \mathcal{P}_g, \quad (20)$$

$$\tilde{P}_y \iff \mathbf{x}_{\text{est}}(0) \in \mathcal{P}_y, \quad (21)$$

where  $\mathbf{x}_{\text{est}}(0)$  is the estimated initial state using  $u_1(t) \equiv a_{\min,1}$  for  $t \in [-\tau_1, 0)$  and  $u_2(t) \equiv a_{\max,2}$  for  $t \in [-\tau_2, 0)$ .

*Proof:* See Appendix D.  $\square$

Theorem 2 suggests that under communication delays, conflict shall be reasoned about using the estimated initial state  $\mathbf{x}_{\text{est}}(0)$ , considering the remote vehicles' worst-case behaviors during the communication delay intervals. Theorem 1 can then be applied to check  $\mathbf{x}_{\text{est}}(0) \in \mathcal{P}_g$  by constructing the opportunity set using  $\mathbf{x}_{\text{est}}(0)$ . This way, although the actual initial state  $\mathbf{x}(0)$  is unknown to the ego vehicle,  $\mathbf{x}(0) \in \mathcal{P}_g$  can be inferred by checking  $\mathbf{x}_{\text{est}}(0) \in \mathcal{P}_g$  since

$$\mathbf{x}_{\text{est}}(0) \in \mathcal{P}_g \implies \mathbf{x}(0) \in \mathcal{P}_g. \quad (22)$$

Note that the reverse direction in (22) does not hold, implying the conservatism in estimating  $\mathbf{x}_{\text{est}}(0)$ . On the other hand, as discussed in the next section, this conservatism can be mitigated when the intent information of remote vehicles is available.

In the rest of this paper, we use  $\tau_1 = \tau_2 = \tau$  for simplicity of presentation, but all results can be easily generalized for  $\tau_1 \neq \tau_2$ . Fig. 3(c)–(d) show conflict charts for the same delay  $\sigma$  in the dynamics as Fig. 3(a)–(b), but with communication delays  $\tau_1 = \tau_2 = \tau = 0.5$  [s]. Here, we use the velocities  $(v_0(0), v_1^{\text{est}}(0), v_2^{\text{est}}(0)) = (27, 28.2, 28.35)$  [m/s], where  $v_1^{\text{est}}(0)$  and  $v_2^{\text{est}}(0)$  are the estimated initial velocities of remote vehicles based on Theorem 2, for the given delayed velocities  $(v_1(-\tau), v_2(-\tau)) = (28.7, 27.85)$  [m/s]. Note that in this example, the actual behaviors of remote vehicles on  $t \in [-\tau, 0)$  are given as  $u_1(t) \equiv 0.6$  [m/s<sup>2</sup>] and  $u_2(t) \equiv 0.3$  [m/s<sup>2</sup>] such that the actual initial velocities  $v_1(0)$  and  $v_2(0)$  are the same as in Fig. 3(a)–(b). In general, the actual behaviors of remote vehicles during the delay time intervals may be given by any (infinitely-many) feasible functions  $u_1(t)$  and  $u_2(t)$  on  $t \in [-\tau, 0)$ , and the delayed status of remote vehicles correspond to these histories. This again reflects the infinite-dimensional nature of time delay systems, which makes the analysis challenging. However, this difficulty is bypassed by the conservatism in our approach, where the worst-case behaviors of remote vehicles are considered over the delay intervals for any given delayed status; see Theorem 2.

We also remark that compared to Fig. 3(a)–(b), the conflict charts under communication delays in Fig. 3(c)–(d) in fact show a different 2D slice of the state space  $\Omega$  corresponding to the estimated initial velocities. Due to conservatism in estimating the remote vehicles' velocities, the 2D slice of no-conflict set  $\mathcal{P}_g$  in  $(h_{10}, h_{02})$ -plane shrinks, while the 2D slice of uncertain set  $\mathcal{P}_y$  expands (although  $\mathcal{P}_g$  and  $\mathcal{P}_y$  remain the same in the 5D state space  $\Omega$ ).

Now we are ready to investigate the effects of communication delay in conflict resolution. The points  $\tilde{A}$ – $\tilde{D}$  in Fig. 3(c)–(d) represent the estimated initial states  $\mathbf{x}_{\text{est}}(0)$  corresponding to the actual initial states A–D in Fig. 3(a)–(b) given the communication delay  $\tau = 0.5$  [s]. The conflict analysis of cases  $\tilde{A}$  and  $\tilde{B}$  are shown in Fig. 4(e)–(h) for the indicated time delays. For the same delay in the dynamics, the additional communication delay makes the opportunity set shrink; cf. Fig. 4(a)–(d). With both delays considered, the opportunity set vanishes for case  $\tilde{A}$ , which corresponds to  $\tilde{A}$  being in the uncertain set  $\mathcal{P}_y$  in Fig. 3(d). In fact, as communication delay increases, the ego vehicle expects a shorter opportunity window for conflict-free lane change, and smaller freedom in choosing proper front and rear gap values to achieve the maneuver. This is summarized in the following corollary.

*Corollary 2.1:* Given delay  $\sigma$  in the dynamics, the ego vehicle's initial status at  $t = 0$ , and the remote vehicles' delayed status at times  $t = -\tau$  and  $t = -\tilde{\tau}$ , where  $0 \leq \tau \leq \tilde{\tau}$ . Let  $\Gamma$  and  $\tilde{\Gamma}$ , and  $T_\Gamma$  and  $\tilde{T}_\Gamma$  be the opportunity sets and their time windows corresponding to communication delays  $\tau$  and  $\tilde{\tau}$ . Then

$$T_\Gamma \supseteq \tilde{T}_\Gamma, \quad |\Gamma(t)| \geq |\tilde{\Gamma}(t)|, \quad \forall t \in T_\Gamma, \quad (23)$$

where  $\Gamma(t)$  and  $\tilde{\Gamma}(t)$  are slices of  $\Gamma$  and  $\tilde{\Gamma}$  at time  $t$ .

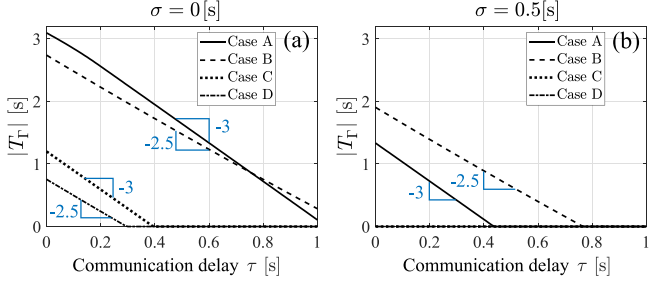


Fig. 6. The length of the opportunity window evaluated as a function of communication delay  $\tau$  for initial state cases A-D and different delays  $\sigma$  in the dynamics of ego vehicle.

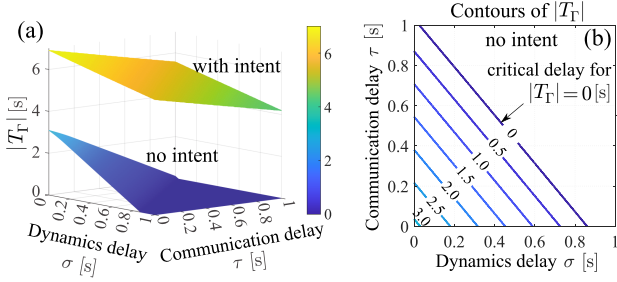


Fig. 7. (a) Length of the opportunity window while varying both delay  $\sigma$  in the dynamics and communication delay  $\tau$  with and without the intent information from remote vehicles for initial state case A. (b) Contours of opportunity window of the lower 3D surface (no-intent case).

This relationship can be shown from the fact that larger communication delay results in more conservative estimated initial state  $\mathbf{x}_{\text{est}}(0)$ . Note that  $\Gamma \supseteq \tilde{\Gamma}$  does not hold in general. Fig. 6(a)–(b) quantify the opportunity window length  $|T_T|$  while varying communication delay  $\tau$  for delays  $\sigma = 0$  and  $0.5$  [s] in the dynamics. Again, increasing communication delay results in the shrinking of the opportunity window at a rate higher than 1, suggesting an amplified effect of communication delay. This again contradicts the intuition that every  $0.1$  [s] of delay results in  $0.1$  [s] degradation of the opportunity window.

The lower 3D surface in Fig. 7(a) illustrates the opportunity window length  $|T_T|$  as a function of delays in both dynamics and communication for initial state case A, while Fig. 7(b) shows the contours of  $|T_T|$  on the  $(\sigma, \tau)$ -plane. The contour  $|T_T| = 0$  gives the critical value combinations of delays  $\sigma$  and  $\tau$  such that the opportunity set disappears, i.e., a conflict-free lane change is no longer guaranteed for larger delay values. We remark that the gradient of the 3-D surface and the critical delay combination indeed depend on the initial states, but the qualitative behaviors remain similar.

In summary, we extended the conflict analysis framework to include time delays in communication by using the estimated initial state as illustrated by Theorem 2. The effects of both delays in vehicle dynamics and communication have been quantified. The next section introduces a V2X connectivity-enabled approach to compensate the negative effects of time delays by utilizing the remote vehicles' intent information.

#### IV. CONFLICT ANALYSIS WITH INTENT INFORMATION

This section extends conflict analysis to the case where the ego vehicle receives the remote vehicles' intent information. We show that intent sharing helps the ego vehicle to predict more accurately the behaviors of the remote vehicles, and thus, facilitates less conservative decision making. Intent information is formally defined as follows.

*Definition 1:* Given the dynamics (1)–(2), the intent of remote vehicle  $i$  is represented by a restricted velocity domain  $v_i(t) \in [\underline{v}_i, \bar{v}_i]$  and acceleration (input) domain  $u_i(t) \in [\underline{a}_i, \bar{a}_i]$  over the time period  $t \in [t_i, t_i + \Delta t_i]$ , where  $v_{\min,i} \leq \underline{v}_i \leq \bar{v}_i \leq v_{\max,i}$ ,  $a_{\min,i} \leq \underline{a}_i \leq \bar{a}_i \leq a_{\max,i}$ , and  $t_i$  is the time when this intent is generated. ■

In the scenario of highway driving, for instance, an intent message may encode the information that the remote vehicle  $i$  will be traveling with velocity between  $\underline{v}_i = 30$  and  $\bar{v}_i = 32$  [m/s], and acceleration between  $\underline{a}_i = -0.5$  and  $\bar{a}_i = 0.8$  [m/s<sup>2</sup>], for the next  $\Delta t_i = 6$  seconds. Note that Definition 1 uses constant bounds for velocity and acceleration in intent information, but our analysis below can be adapted to the case where these bounds are time-varying.

As with status information, we assume that the ego vehicle receives intent information from remote vehicles in a synchronized manner. Intent information can also have communication delay; see Fig. 2. For example, if intent information from vehicle  $i$  is received at time  $t = 0$  with communication delay  $\tau_i$ , then the time domain where this intent remains valid is  $t \in [-\tau_i, \Delta t_i - \tau_i]$ . When intent information is received together with status information, Theorem 2 still holds when estimating the initial state  $\mathbf{x}_{\text{est}}(0)$  using

$$u_1(t) = \begin{cases} \underline{a}_1, & \text{if } t \in [-\tau_1, \min\{0, \Delta t_1 - \tau_1\}], \\ a_{\min,1}, & \text{if } t \in [\min\{0, \Delta t_1 - \tau_1\}, 0], \end{cases} \quad (24)$$

$$u_2(t) = \begin{cases} \bar{a}_2, & \text{if } t \in [-\tau_2, \min\{0, \Delta t_2 - \tau_2\}], \\ a_{\max,2}, & \text{if } t \in [\min\{0, \Delta t_2 - \tau_2\}, 0], \end{cases} \quad (25)$$

which represents the remote vehicles' worst behaviors on the communication delay intervals under the given intent information. Notice that intent information leads to less conservative estimation  $\mathbf{x}_{\text{est}}(0)$ . Similarly, Lemma 1 and Theorem 1 still hold when replacing  $u_1(t) \equiv a_{\min,1}$  and  $u_2(t) \equiv a_{\max,2}$  with

$$u_1(t) = \begin{cases} \underline{a}_1, & \text{if } t \in [0, \max\{0, \Delta t_1 - \tau_1\}], \\ a_{\min,1}, & \text{otherwise,} \end{cases} \quad (26)$$

$$u_2(t) = \begin{cases} \bar{a}_2, & \text{if } t \in [0, \max\{0, \Delta t_2 - \tau_2\}], \\ a_{\max,2}, & \text{otherwise,} \end{cases} \quad (27)$$

which correspond to the worst future motion of remote vehicles based on the intent. Note that intent information improves the ego vehicle's prediction on the remote vehicles' motions, while the delay in the ego vehicle's dynamics can be similarly handled as in Theorem 1. Thus, the conflict analysis framework built in the previous section can be still applied.

Denoting the no-conflict, uncertain, and conflict sets under intent information as  $\bar{\mathcal{P}}_g$ ,  $\bar{\mathcal{P}}_y$ , and  $\bar{\mathcal{P}}_r$ , the following relationships can be derived:

$$\mathcal{P}_g \subseteq \bar{\mathcal{P}}_g, \quad \mathcal{P}_y \supseteq \bar{\mathcal{P}}_y, \quad \mathcal{P}_r = \bar{\mathcal{P}}_r = \emptyset. \quad (28)$$

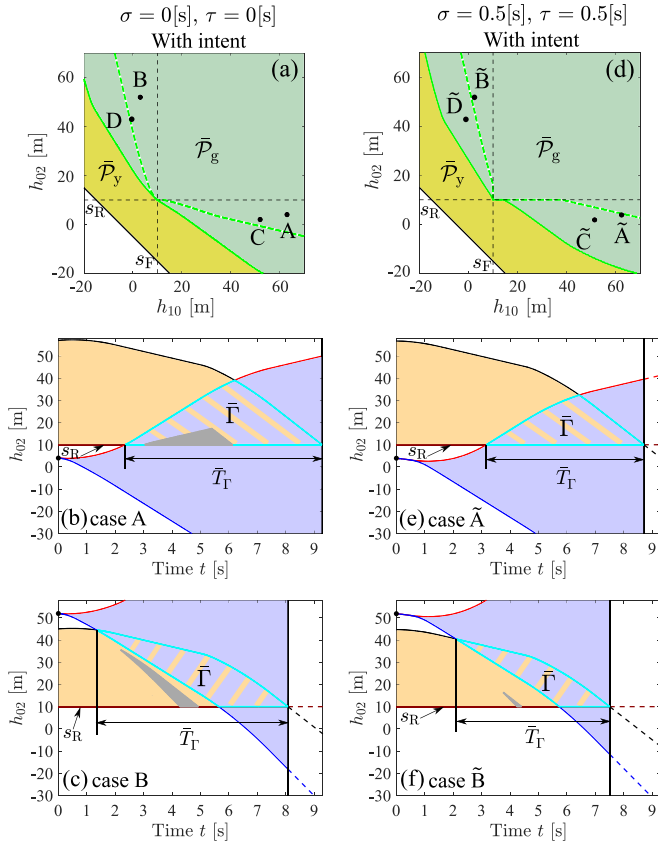


Fig. 8. Conflict analysis with intent  $v_1(t), v_2(t) \in [27, 30]$  [m/s],  $u_1(t), u_2(t) \in [-1, 1]$  [m/s<sup>2</sup>], and  $\Delta t_1 = \Delta t_2 = 5$  [s]. (a)-(c) Conflict chart and opportunity set without time delays for the same initial velocities as in Fig. 3(a). (d)-(f) Conflict chart and opportunity set with delay in dynamics  $\sigma = 0.5$  [s] and communication delay  $\tau = 0.5$  [s]. The gray regions indicate the corresponding opportunity sets in Fig. 4(a)-(b) and (g)-(h) without intent.

This reveals that the green no-conflict set expands and the yellow uncertain set shrinks due to the intent; see the conflict charts in Fig. 8(a) and (d) where the dashed green boundaries correspond to the no-intent case in Fig. 3(a) and (d). A large portion of the originally yellow domain converts to green, indicating the ego vehicle's increased confidence in deciding to change lane.

Furthermore, given the time delays, the initial status of the ego vehicle, and the delayed status of the remote vehicles, the opportunity set  $\bar{\Gamma}$  and the opportunity window  $\bar{T}_\Gamma$  under intent information satisfy

$$T_\Gamma \subseteq \bar{T}_\Gamma, \quad |\Gamma(t)| \leq |\bar{\Gamma}(t)|, \quad \forall t \in T_\Gamma, \quad (29)$$

where  $\Gamma$  and  $T_\Gamma$  correspond to the no-intent case. This suggests that an enlarged opportunity window is now accessible for the ego vehicle because of the intent information. This is illustrated in Fig. 8(b)-(c) for initial states A and B and in Fig. 8(e)-(f) for initial states  $\tilde{A}$  and  $\tilde{B}$ . The gray regions mark the opportunity sets without intent information; cf. Fig. 4(a)-(b) and (g)-(h). Notice that with intent the opportunity set of case  $\tilde{A}$  is no longer empty, since the enlarged green (no-conflict) set now contains the point  $\tilde{A}$  in Fig. 8(d). The methodology developed in Section III still enables the computation of the opportunity set  $\bar{\Gamma}$  as detailed in Appendix B.

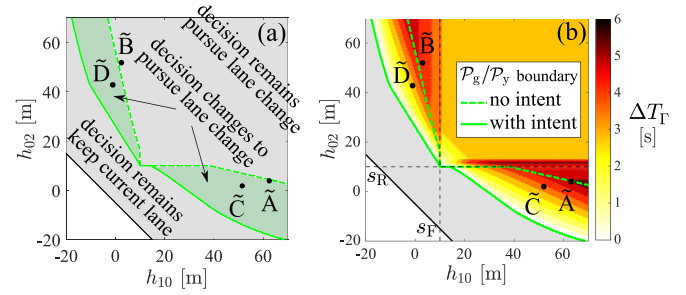


Fig. 9. (a) Chart showing the decision change under the same intent information, time delays, and estimated initial velocities as in Fig. 8(d)-(f). (b) Heat map of opportunity window expansion  $\Delta T_\Gamma = |\bar{T}_\Gamma| - |T_\Gamma|$ .

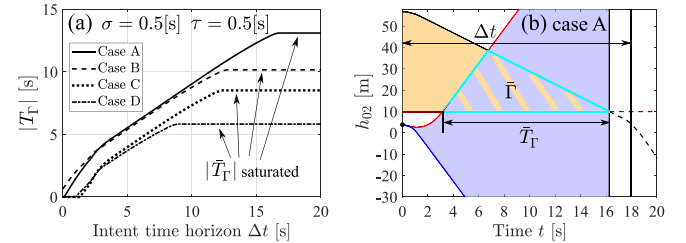


Fig. 10. (a) Length of the opportunity window as a function of intent horizon for initial state cases A-D and time delays indicated. (b) Mechanism behind the saturation of the opportunity window.

We quantify the benefits of intent with respect to decision making in Fig. 9. Panel (a) is obtained by superimposing the conflict chart in Figs. 8(d) and 3(d). Regions where ego vehicle's decision regarding lane change changes are shaded green. The heat map in panel (b) quantifies the growth of the opportunity window  $\Delta T_\Gamma = |\bar{T}_\Gamma| - |T_\Gamma|$  due to intent. We can observe an ubiquitous increase of the opportunity window inside the set  $\bar{P}_g$ , while substantial benefits are gained around the boundary dividing the sets  $\bar{P}_g$  and  $\bar{P}_y$ . Note that even though we used the intent horizon  $\Delta t_1 = \Delta t_2 = 5$  [s] the opportunity window expands more than 5 [s] for some initial states. Even in the region where the decision remains pursuing lane change, the opportunity window increases.

The upper 3D surface in Fig. 7(a) quantifies the opportunity window length as a function of the time delays under the intent information for initial state case A. Apart from increasing the value of opportunity window, intent information also reduces the opportunity window's degradation rate as time delays increase; notice the milder slope of the upper surface compared to the lower one.

In Fig. 10(a) we highlight the effect of the intent horizon  $\Delta t_1 = \Delta t_2 = \Delta t$  on the length of the opportunity window  $|\bar{T}_\Gamma|$ . Initially, the opportunity window increases with the intent horizon with a rate higher than 1, and then eventually saturates for higher  $\Delta t$  values. The first slope change at  $\Delta t \approx 2.5$  [s] corresponds to speed limit being reached inside the intent horizon. The saturation of  $|\bar{T}_\Gamma|$  suggests that the benefit of increasing intent horizon is bounded. This is illustrated in Fig. 10(b) where the intent horizon  $\Delta t$  exceeds the length of the opportunity window  $\bar{T}_\Gamma$ . We remark that for intent information with less

restricted velocity and acceleration bounds, the opportunity window length  $|\bar{T}_\Gamma|$  saturates at a smaller value for shorter horizon  $\Delta t$ . We also remark that in our intent definition the velocity and acceleration bounds remain unchanged during the intent horizon  $\Delta t$ . However, our theories and numerical tools can be adapted to the case where the remote vehicles update their intent within the  $\Delta t$  horizon. This is outside the scope of this paper and left as our future work.

In this section, we extended conflict analysis for the case when the remote vehicles' intent is available. We showed that intent information can significantly increase the ego vehicle's capability for a conflict-free maneuver and compensate for the shrink of the opportunity set caused by time delays. Using the theories developed so far, the next section discusses controller design and presents simulation results to demonstrate the power of the developed framework.

## V. CONTROLLER DESIGN AND SIMULATION

In this section, a controller is designed for the ego vehicle to secure the required longitudinal distances for a non-conflicting lane change with time delays in both dynamics and communication. Feeding real highway data into numerical simulations, we validate the effectiveness of the extended conflict analysis framework and demonstrate the benefits of intent sharing.

### A. Goal-Oriented Control

For  $\mathbf{x}(0) \in \mathcal{P}_g$  (or  $\mathbf{x}_{\text{est}}(0) \in \mathcal{P}_g$  under communication delay), we have a non-empty opportunity set  $\Gamma \neq \emptyset$  and each point in this set  $(t, h_{02}) \in \Gamma$  provides a feasible rear gap and a corresponding time. Securing such rear gap simultaneously guarantees the formation of the required front gap. Therefore, one can design the control input  $u_0(t)$  by selecting an appropriate goal point  $(t^G, h_{02}^G) \in \Gamma$  for the ego vehicle to pursue. We refer to this as goal-oriented control. We emphasize that the existence of such control input  $u_0(t)$  is guaranteed by the non-empty opportunity set  $\Gamma$ . One may design  $u_0(t)$  to realize a variety of desired performances of the ego vehicle, e.g., optimal time efficiency and/or energy efficiency.

From the robustness perspective, we choose the goal point to be the "center" of the opportunity set, that is, we select  $t^G$  in the middle of  $T_\Gamma$  and  $h_{02}^G$  in the middle of the slice  $\Gamma(t^G)$ ; see the black dots in Fig. 11(a) and (e). Under time delays in both dynamics and communication, we propose a goal-oriented control input of constant value, i.e.,  $u_0(t) = u_0^G$ , with which the goal point  $(t^G, h_{02}^G) \in \Gamma$  can be pursued by the ego vehicle. Appendix E gives the analytical expression of  $u_0^G$ . Under this constant-value input, the expected trajectory  $h_{02}(t)$  is illustrated in Fig. 11(a) and (e) by gray arrows. Notice that the goal-oriented controller automatically guarantees the invariance of domain  $\mathcal{P}_g$  (or  $\bar{\mathcal{P}}_g$  when intent is shared) independent of the future motions of remote vehicles. If the ego vehicle receives the remote vehicles' updated status and intent information, it may recompute the opportunity set  $\Gamma$ , update the goal point  $(t^G, h_{02}^G) \in \Gamma$ , and recalculate the corresponding goal-oriented control input  $u_0^G$ ; see Fig. 11(b)–(d) and (f)–(h). Simulation results in the next subsection demonstrate that the ego vehicle's passenger comfort

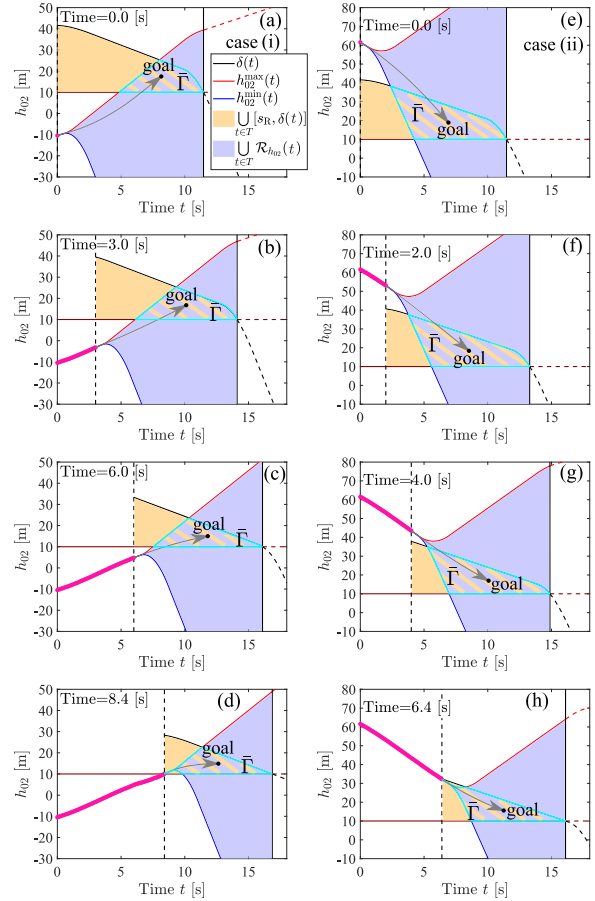


Fig. 11. Evolution of opportunity set  $\bar{\Gamma}$ , goal point, and trajectory  $h_{02}^{\text{est}}(t)$  under delay  $\sigma = 0.5$  [s] in the ego vehicle's dynamics, and communication delay  $\tau = 0.1$  [s], with intent information  $v_1 \in [34.9, 36.7]$  [m/s],  $v_2 \in [36.5, 37.2]$  [m/s],  $u_1 \in [-0.6, 0.4]$  [m/s<sup>2</sup>],  $u_2 \in [-1.5, 0.5]$  [m/s<sup>2</sup>],  $\Delta t_1 = \Delta t_2 = 10$  [s]. The goal-oriented controller  $u_0(t) = u_0^G$  is used with status and intent updates every 0.1 [s]. (a)–(d) Case (i) where the ego vehicle is initially traveling behind the remote vehicles. (e)–(h) Case (ii) where the ego vehicle is initially traveling in front of the remote vehicles.

and time efficiency can benefit from the frequent status and intent updates.

### B. Simulations With Real Highway Data

We represent the remote vehicles' motion by utilizing real data recorded on human-driven vehicles involved in a lane change scenario on highway I-94 in southeast Michigan. In this maneuver, the front remote vehicle 1 was decelerating while the rear remote vehicle 2 was accelerating and it traveled faster than vehicle 1; see the speed and acceleration data in Fig. 12(a)–(b) and (c). This represents an adversarial scenario where the two remote vehicles were shortening the distance between them; see the gap  $h_{12}$  in Fig. 12(c) and (f). The ego vehicle is assumed to be a connected automated vehicle which attempts to enter the target lane between the remote human-driven vehicles. We consider the delay in the ego vehicle's dynamics to be  $\sigma = 0.5$  [s], while the communication delays associated with both remote vehicles to be  $\tau = 0.1$  [s].

TABLE II  
MANEUVER RESULTS UNDER DIFFERENT V2X CONDITIONS

V2X condition	Status sharing only	Status and intent sharing 1 [s] update rate	Status and intent sharing 0.1 [s] update rate
Maneuver result case (i)	Lane change opportunity missed	Lane change opportunity secured Maneuver time 9.0 [s]	Lane change opportunity secured Maneuver time 8.4 [s]
Maneuver result case (ii)	Lane change opportunity missed	Lane change opportunity secured Maneuver time 7.0 [s]	Lane change opportunity secured Maneuver time 6.4 [s]

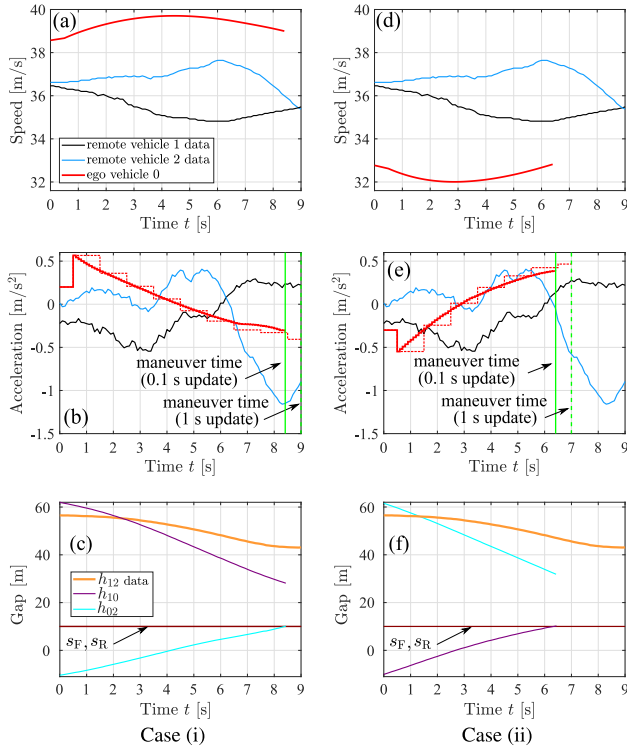


Fig. 12. Simulation results under the same time delays, initial states, and intent as in Fig. 11. (a)–(c) Results for case (i). (d)–(f) Results for case (ii). The dashed magenta curves in (b) and (e) correspond to status and intent updates every 1 [s].

At time  $t = 0$ , the remote vehicles have initial states  $(r_1(0), r_2(0)) = (61.52, 0)$  [m] and  $(v_1(0), v_2(0)) = (36.46, 36.62)$  [m/s]. Here, without loss of generality, we set the initial position of remote vehicle 2 as the origin. For the ego vehicle, we consider two different initial states. In case (i) we set  $r_0(0) = -5.43$  [m] and  $v_0(0) = 38.57$  [m/s], that is, the ego vehicle initially travels behind the remote vehicles; while in case (ii) we set  $r_0(0) = 66.57$  [m] and  $v_0(0) = 32.77$  [m/s], that is, the ego vehicle initially travels in front of the remote vehicles. Note that at  $t = 0$  the ego vehicle only has access to the remote vehicles' delayed status  $(r_1(-0.1), r_2(-0.1)) = (57.95, -3.64)$  [m] and  $(v_1(-0.1), v_2(-0.1)) = (36.46, 36.62)$  [m/s], and it is necessary to estimate their current status based on Theorem 2. Here, we use  $(v_{\max,0}, v_{\max,1}, v_{\max,2}) = (42, 40, 40)$  [m/s] as speed limits corresponding to highway driving, while other parameters remain unchanged as in Table I. This adapts the conflict analysis to the driving scenario considered.

With status-sharing information only, the estimated initial state is such that  $\mathbf{x}_{\text{est}}(0) \in \mathcal{P}_y$  holds for both cases (i) and (ii), and thus, status information does not provide the ego

vehicle with enough confidence for pursuing the lane change. Therefore, the chance to change lanes may be missed if the remote vehicles share only their status. However, the ego vehicle's decision can be improved when intent information is shared. The remote vehicles' intent can be extracted from the data as  $v_1(t) \in [34.9, 36.7]$  [m/s],  $u_1(t) \in [-0.6, 0.4]$  [m/s<sup>2</sup>],  $v_2(t) \in [36.5, 37.2]$  [m/s], and  $u_2(t) \in [-1.5, 0.5]$  [m/s<sup>2</sup>]. This yields the estimated initial speeds  $(v_1^{\text{est}}(0), v_2^{\text{est}}(0)) = (36.4, 36.67)$  [m/s] and the estimated initial front and rear gaps  $(h_{10}^{\text{est}}(0), h_{02}^{\text{est}}(0)) = (62.03, -10.45)$  [m] for case (i), and  $(h_{10}^{\text{est}}(0), h_{02}^{\text{est}}(0)) = (-9.97, 61.55)$  [m] for case (ii), assuming the intent of both vehicles covers  $\Delta t_1 = \Delta t_2 = 10$  [s]. This leads to  $\bar{\mathbf{x}}_{\text{est}}(0) \in \bar{\mathcal{P}}_g$  for both cases. Accordingly, the decision of changing lane is made by the ego vehicle, and executed by the goal-oriented controller  $u_0(t) = u_0^G$ . Note that the value of input  $u_0^G$  is updated each time the ego vehicle receives a status and/or intent information update.

Fig. 11(a)–(d) illustrate the evolution of opportunity set  $\bar{\Gamma}$ , the goal point  $(t^G, h_{02}^G) \in \bar{\Gamma}$ , and the trajectory  $h_{02}^{\text{est}}(t)$  (magenta curve) with status and intent updates in every 0.1 [s] for case (i). Panels (e)–(h) show the corresponding evolution for case (ii). Notice that when intent is updated, its horizon is extended, but the bounds of velocity and acceleration do not change. At  $t = 8.4$  [s] and  $t = 6.4$  [s] for cases (i) and (ii), respectively, the required rear gap (and front gap) are already formed by the ego vehicle. This can be confirmed by noticing that  $(t, h_{02}^{\text{est}}(t)) \in \bar{\Gamma}$  holds, and thus,  $\mathbf{x}(t) \in \mathcal{P}_g$  holds according to (22). Then, the ego vehicle can initiate the lateral lane change motion immediately without further pursuing the goal point. Thus, goal point is functioning as a guidance for the motion of ego vehicle until sufficient relative distances are formed, while it is not necessary to actually reach it.

Fig. 12(a)–(b) and (d)–(e) depict the ego vehicle's time profiles by solid red curves for update rates 0.1 [s] and 1 [s], respectively. Notice that when the ego vehicle receives status and intent updates less frequently, conflict-free lane change can still be performed but the required front and rear distances are secured at a later time, at  $t = 9.0$  [s] and  $t = 7.0$  [s] for cases (i) and (ii), respectively. Also, less smooth control command is prescribed as shown in the dashed red curves. Therefore, by receiving updated status and intent information frequently, the ego vehicle can significantly improve its time efficiency and passenger comfort. Table II summarizes these results.

## VI. CONCLUSION

This paper presented a conflict analysis framework for multiple vehicles possessing different levels of automation in cooperative maneuvering, under time delays in vehicle dynamics and V2X communication. The merits of communication in conflict

prevention were examined in the presence of delays by conducting conflict analysis. In particular, we considered status-sharing and intent-sharing communication. The effects of time delays on conflicts in a mixed-autonomy environment were systematically studied and quantified. It was revealed that conflict-free maneuvers can be facilitated by receiving status information, but time delays can compromise such opportunities. It was also shown that receiving intent information compensates the effects of delays, removes the conservatism from decision making, and improves efficiency of controllers of connected vehicles. A goal-oriented controller was designed for a connected automated vehicle to guarantee conflict-free maneuvers, and the benefits of different types of V2X information exchange were demonstrated via real highway data-based simulations. It is shown that receiving the remote vehicles' status and intent information more frequently further benefits the passenger comfort and time efficiency of the connected automated vehicle.

As future work, we will use more detailed models of vehicle dynamics and optimize the goal-oriented controllers based on different metrics such as time, energy efficiency, and passenger comfort. Moreover, we plan to experimentally validate the developed conflict analysis framework using real vehicles, while implementing intent-sharing communication on commercially available radios. Other extensions of the work include exploring cooperative maneuvers where planned paths and specific control laws (control structures and parameters) are agreed upon between connected vehicles prior to execution. This will allow us to extend our framework to higher levels of cooperation.

#### APPENDIX A PROOF OF LEMMA 1

( $\Rightarrow$ ). The left hand side of (13) implies that for  $(u_1, u_2) \equiv (a_{\min,1}, a_{\max,2})$ , one has  $\exists u_0, \exists t \geq 0, h_{10}(t) \geq s_F \wedge h_{02}(t) \geq s_R$ . Therefore,  $h_{12}(t) = h_{10}(t) + h_{02}(t) + l \geq s_F + s_R + l$ , implying that  $t \in T$  is satisfied by such  $t$ .

( $\Leftarrow$ ). The right hand side of (13) implies that for  $(u_1, u_2) \equiv (a_{\min,1}, a_{\max,2})$ , one has  $\exists u_0, P$ . Let  $u_0^*$  and  $t^*$  be an input  $u_0$  and a time  $t$  such that  $h_{10}(t^*) \geq s_F \wedge h_{02}(t^*) \geq s_R$  under  $(u_1, u_2) \equiv (a_{\min,1}, a_{\max,2})$ . For  $(u_1, u_2) \neq (a_{\min,1}, a_{\max,2})$ , even larger  $h_{10}$  and  $h_{02}$  values are generated by the same input  $u_0^*$  at  $t^*$ , that is,  $h_{10}(t^*) \geq s_F \wedge h_{02}(t^*) \geq s_R$  still holds. Therefore,  $\forall u_1, \forall u_2, \exists u_0, P$ .

#### APPENDIX B ANALYTICAL FORMS OF $\delta(t)$ , $h_{02}^{\min}(t)$ , AND $h_{02}^{\max}(t)$

With status information only, one has  $\delta(t) = r_1^*(t) - r_2^*(t) - s_F - 2l$ , where

$$r_1^*(t) = g(r_1(0), v_1(0), a_{\min,1}, v_{\min,1}, v_{\max,1}, t), \quad (30)$$

$$r_2^*(t) = g(r_2(0), v_2(0), a_{\max,2}, v_{\min,2}, v_{\max,2}, t), \quad (31)$$

and the function  $g(r(0), v(0), a, v_{\min}, v_{\max}, t)$  is defined as

i) For  $a > 0$ ,

$$g(r(0), v(0), a, v_{\min}, v_{\max}, t)$$

$$= \begin{cases} r(0) + v(0)t + \frac{1}{2}at^2 & \text{if } t \leq \frac{(v_{\max} - v(0))}{a}, \\ r(0) - \frac{(v_{\max} - v(0))^2}{2a} + v_{\max}t & \text{otherwise,} \end{cases} \quad (32)$$

ii) For  $a = 0$ ,

$$g(r(0), v(0), a, v_{\min}, v_{\max}, t) = r(0) + v(0)t, \quad (33)$$

iii) For  $a < 0$ ,

$$g(r(0), v(0), a, v_{\min}, v_{\max}, t) = \begin{cases} r(0) + v(0)t + \frac{1}{2}at^2 & \text{if } t \leq \frac{(v_{\min} - v(0))}{a}, \\ r(0) - \frac{(v_{\min} - v(0))^2}{2a} + v_{\min}t & \text{otherwise,} \end{cases} \quad (34)$$

and  $h_{02}^{\min}(t) = \underline{r}_0^*(t) - r_2^*(t) - l$ ,  $h_{02}^{\max}(t) = \bar{r}_0^*(t) - r_2^*(t) - l$ , where

$$\underline{r}_0^*(t) = \begin{cases} \tilde{g}(r_0(0), v_0(0), t) & \text{if } t \leq \sigma, \\ g(r_0(\sigma), v_0(\sigma), a_{\min,0}, v_{\min,0}, v_{\max,0}, t - \sigma) & \text{otherwise,} \end{cases} \quad (35)$$

$$\bar{r}_0^*(t) = \begin{cases} \tilde{g}(r_0(0), v_0(0), t) & \text{if } t \leq \sigma, \\ g(r_0(\sigma), v_0(\sigma), a_{\max,0}, v_{\min,0}, v_{\max,0}, t - \sigma) & \text{otherwise,} \end{cases} \quad (36)$$

$$\tilde{g}(r_0(0), v_0(0), t) = r_0(0) + v_0(0)t + \int_0^t \int_0^{\bar{t}} \text{sat}(u(\bar{t} - \sigma)) d\bar{t} d\bar{t}, \quad (37)$$

$$r_0(\sigma) = \tilde{g}(r_0(0), v_0(0), \sigma), \quad (38)$$

$$v_0(\sigma) = v_0(0) + \int_0^\sigma \text{sat}(u(\bar{t} - \sigma)) d\bar{t}. \quad (39)$$

Note that for  $t \in [0, \sigma]$ ,  $u(t - \sigma)$  represents the control command history of the ego vehicle, and thus, is a given deterministic function.

Under remote vehicles' intent, one shall calculate  $\delta(t)$ ,  $h_{02}^{\min}(t)$ , and  $h_{02}^{\max}(t)$  in a similar way utilizing the previously given formulae, where  $r_1^*(t)$  and  $r_2^*(t)$  need to be updated as

$$r_1^*(t) = \begin{cases} g(r_1(0), v_1(0), \underline{a}_1, \underline{v}_1, \bar{v}_1, t) & \text{if } t \leq \Delta t_1, \\ g(r_1^*(\Delta t_1), v_1^*(\Delta t_1), a_{\min,1}, v_{\min,1}, v_{\max,1}, t - \Delta t_1) & \text{otherwise,} \end{cases} \quad (40)$$

$$r_2^*(t) = \begin{cases} g(r_2(0), v_2(0), \bar{a}_2, \underline{v}_2, \bar{v}_2, t) & \text{if } t \leq \Delta t_2, \\ g(r_2^*(\Delta t_2), v_2^*(\Delta t_2), a_{\max,2}, v_{\min,2}, v_{\max,2}, t - \Delta t_2) & \text{otherwise,} \end{cases} \quad (41)$$

where  $v_1^*(\Delta t_1) = \max\{v_1(0) + \underline{a}_1 \Delta t_1, \underline{v}_1\}$  and  $v_2^*(\Delta t_2) = \min\{v_2(0) + \bar{a}_2 \Delta t_2, \bar{v}_2\}$ .

Notice that under communication delay, one needs to replace  $r_1(0)$ ,  $v_1(0)$ ,  $r_2(0)$ , and  $v_2(0)$  in (30), (31), (40), and (41) with their estimated values based on Theorem 2.

APPENDIX C  
PROOF OF THEOREM 1

If  $\Gamma \neq \emptyset$ , then according to the definition of  $\Gamma$  in (14), under  $(u_1, u_2) \equiv (a_{\min,1}, a_{\max,2})$ , one has  $\exists u_0, \exists t \in T, s_R \leq h_{02}(t) \leq \delta(t)$ . Substituting  $\delta(t) = h_{12}(t) - s_F - l$  gives  $h_{02}(t) \leq h_{12}(t) - s_F - l$ , i.e.,  $s_F \leq h_{10}(t)$ . These and Lemma 1 yield  $\mathbf{x}(0) \in \mathcal{P}_g$ .

If  $\Gamma = \emptyset$ , then under  $(u_1, u_2) \equiv (a_{\min,1}, a_{\max,2})$ , one has  $\forall u_0(t), \forall t \in T, \neg\{s_R \leq h_{02}(t) \leq \delta(t)\}$ , i.e.,  $\neg\{h_{10}(t) \geq s_F \wedge h_{02}(t) \geq s_R\}$ . Also,  $\forall t \notin T$  one still obtains  $\neg\{h_{10}(t) \geq s_F \wedge h_{02}(t) \geq s_R\}$ . Therefore, for  $(u_1, u_2) \equiv (a_{\min,1}, a_{\max,2})$ ,  $\forall u_0, \neg P$ . This yields  $\mathbf{x}(0) \notin \mathcal{P}_g$ .

APPENDIX D  
PROOF OF THEOREM 2

By noting that  $\mathbf{x}_{\text{est}}(0) \in \mathcal{P}_g$  is equivalent to  $\{u_1(t) \equiv a_{\min,1}, t \in [-\tau_1, 0], u_2(t) \equiv a_{\max,2}, t \in [-\tau_2, 0], \forall u_1(t), t > 0, \forall u_2(t), t > 0, \exists u_0(t), t > 0, P\}$ ,  $\tilde{P}_g \implies \mathbf{x}_{\text{est}}(0) \in \mathcal{P}_g$  is obvious based on the definition of  $\tilde{P}_g$  in (17).

If  $\mathbf{x}_{\text{est}}(0) \in \mathcal{P}_g$  holds, let  $u_0^*$  and  $t^*$  be an input  $u_0$  and a time  $t$  such that the proposition  $P$  holds, i.e.,  $h_{10}(t^*) \geq s_F \wedge h_{02}(t^*) \geq s_R$ . Then,  $\forall u_1(t) \neq a_{\min,1}, t \in [-\tau_1, 0], \forall u_2(t) \neq a_{\max,2}, t \in [-\tau_2, 0]$ , at time  $t^*$  even larger  $h_{10}$  and  $h_{02}$  values are obtained by the same input  $u_0^*$ , that is,  $h_{10}(t^*) \geq s_F \wedge h_{02}(t^*) \geq s_R$  still holds. Thus,  $\tilde{P}_g \longleftarrow \mathbf{x}_{\text{est}}(0) \in \mathcal{P}_g$ . These give (20).

On the other hand, (21) is obtained from (20) by noting that  $\tilde{P}_y = \neg\tilde{P}_g \wedge \neg\tilde{P}_r = \neg\tilde{P}_g \wedge \text{True} = \neg\tilde{P}_g$  and  $\mathbf{x}_{\text{est}}(0) \in \mathcal{P}_y \iff \mathbf{x}_{\text{est}}(0) \notin \mathcal{P}_g$ .

These complete the proof of Theorem 2.

APPENDIX E  
GOAL-ORIENTED CONTROLLER  $u_0^G$

Given a goal point  $(t^G, h_{02}^G) \in \Gamma$  (or  $\bar{\Gamma}$ ), we have

$$u_0^G = \begin{cases} \frac{2(s^G - (t^G - \sigma)v_0)}{(t^G - \sigma)^2}, & \text{if } s^G \in \left[ \frac{(t^G - \sigma)(v_0 + v_{\min,0})}{2}, \frac{(t^G - \sigma)(v_0 + v_{\max,0})}{2} \right], \\ f_1(v_0, t^G, s^G), & \text{if } s^G \in [0, \frac{(t^G - \sigma)(v_0 + v_{\min,0})}{2}], \\ f_2(v_0, t^G, s^G), & \text{otherwise.} \end{cases} \quad (42)$$

Here,  $v_0$  represents  $v_0(\sigma)$  given in (39), and  $s^G$  represents the distance that the ego vehicle shall travel for  $t > \sigma$  to form the rear gap  $h_{02}^G$  at  $t^G$  considering the remote vehicle 2's worst-case behavior. Thus,  $s^G = r_2^*(t^G) - r_0(\sigma) + h_{02}^G + l$  for the  $r_2^*(\cdot)$  in (31) or (41) depending on whether intent of remote vehicle 2 is available, and  $r_0(\sigma)$  in (38).

$$f_1(v_0, t^G, s^G) = \begin{cases} \frac{2(s^G - (t^G - \sigma)v_0)}{(t^G - \sigma)^2}, & \text{if } a_{\min,0} \geq \frac{v_{\min,0} - v_0}{t^G - \sigma}, \\ \frac{(v_0 - v_{\min,0})^2}{2((t^G - \sigma)v_{\min,0} - s^G)}, & \text{otherwise,} \end{cases} \quad (43)$$

$$f_2(v_0, t^G, s^G) = \begin{cases} \frac{2(s^G - (t^G - \sigma)v_0)}{(t^G - \sigma)^2}, & \text{if } a_{\max,0} \leq \frac{v_{\max,0} - v_0}{t^G - \sigma}, \\ \frac{(v_0 - v_{\max,0})^2}{2((t^G - \sigma)v_{\max,0} - s^G)}, & \text{otherwise.} \end{cases} \quad (44)$$

Notice that in (42), we divide  $u_0^G$  into three cases to deal with the speed saturation of the ego vehicle as it travels distance  $s^G$  during the time interval  $(\sigma, t^G]$ .

REFERENCES

- [1] L. Hobert, A. Festag, I. Llatser, L. Altomare, F. Visintainer, and A. Kovacs, "Enhancements of V2X communication in support of cooperative autonomous driving," *IEEE Commun. Mag.*, vol. 53, no. 12, pp. 64–70, Dec. 2015.
- [2] I. Llatser, T. Michalke, M. Dolgov, F. Wildschütte, and H. Fuchs, "Cooperative automated driving use cases for 5G V2X communication," in *Proc. IEEE 2nd 5G World Forum*, 2019, pp. 120–125.
- [3] J. Jeong et al., "A comprehensive survey on vehicular networks for smart roads: A focus on IP-based approaches," *Veh. Commun.*, vol. 29, 2021, Art. no. 100334.
- [4] C. Liu, C.-W. Lin, S. Shiraishi, and M. Tomizuka, "Distributed conflict resolution for connected autonomous vehicles," *IEEE Trans. Intell. Veh.*, vol. 3, no. 1, pp. 18–29, Mar. 2020.
- [5] J. Rios-Torres and A. A. Malikopoulos, "A survey on the coordination of connected and automated vehicles at intersections and merging at highway on-ramps," *IEEE Trans. Intell. Transp. Syst.*, vol. 18, no. 5, pp. 1066–1077, May 2017.
- [6] R. Hult, M. Zanon, S. Gros, and P. Falcone, "Optimal coordination of automated vehicles at intersections: Theory and experiments," *IEEE Trans. Control Syst. Technol.*, vol. 27, no. 6, pp. 2510–2525, Nov. 2019.
- [7] A. I. M. Medina, N. van de Wouw, and H. Nijmeijer, "Automation of a T-intersection using virtual platoons of cooperative autonomous vehicles," in *Proc. 18th Int. Conf. Intell. Transp. Syst.*, Las Palmas, Spain, 2015, pp. 1696–1701.
- [8] R. Kianfar, P. Falcone, and J. Fredriksson, "Safety verification of automated driving systems," *IEEE Intell. Transp. Syst. Mag.*, vol. 5, no. 4, pp. 73–86, Winter 2013.
- [9] M. R. Hafner, D. Cunningham, L. Caminiti, and D. Del Vecchio, "Cooperative collision avoidance at intersections: Algorithms and experiments," *IEEE Trans. Intell. Transp. Syst.*, vol. 14, no. 3, pp. 1162–1175, Sep. 2013.
- [10] S. Bansal, M. Chen, S. Herbert, and C. J. Tomlin, "Hamilton-Jacobi reachability: A brief overview and recent advances," in *Proc. IEEE 56th Conf. Decis. Control*, Melbourne, Australia, 2017, pp. 2242–2253.
- [11] *Taxonomy and Definitions for Terms Related to Cooperative Driving Automation for On-Road Motor Vehicles*, SAE Int., SAE Standard J3216, 2020.
- [12] *Taxonomy and Definitions for Terms Related to Driving Automation Systems for On-Road Motor Vehicles*, SAE Int., SAE Standard J3016, 2021.
- [13] Y. E. Sahin, Z. Liu, K. Rutledge, D. Panagou, S. Z. Yong, and N. Ozay, "Intention-aware supervisory control with driving safety applications," in *Proc. IEEE Conf. Control Technol. Appl.*, 2019, pp. 1–8.
- [14] M. Koschi and M. Althoff, "Set-based prediction of traffic participants considering occlusions and traffic rules," *IEEE Trans. Intell. Veh.*, vol. 6, no. 2, pp. 249–265, Jun. 2021.
- [15] B. M. Albaba and Y. Yildiz, "Modeling cyber-physical human systems via an interplay between reinforcement learning and game theory," *Annu. Rev. Control*, vol. 48, pp. 1–21, 2019.
- [16] M. Karimi, C. Roncoli, C. Alecsandru, and M. Papageorgiou, "Cooperative merging control via trajectory optimization in mixed vehicular traffic," *Transp. Res. C: Emerg. Technol.*, vol. 116, 2020, Art. no. 102663.
- [17] J. Guo, S. Cheng, and Y. Liu, "Merging and diverging impact on mixed traffic of regular and autonomous vehicles," *IEEE Trans. Intell. Transp. Syst.*, vol. 22, no. 3, pp. 1639–1649, Mar. 2021.
- [18] H. M. Wang, T. G. Molnár, S. S. Avedisov, A. H. Sakr, O. Altintas, and G. Orosz, "Conflict analysis for cooperative merging using V2X communication," in *Proc. IEEE Intell. Veh. Symp.*, 2020, pp. 1538–1543.
- [19] H. M. Wang, S. S. Avedisov, A. H. Sakr, O. Altintas, and G. Orosz, "Opportunistic strategy for cooperative maneuvering using conflict analysis," in *Proc. IEEE Intell. Veh. Symp.*, 2021, pp. 348–353.
- [20] H. M. Wang, S. S. Avedisov, T. G. Molnár, A. H. Sakr, O. Altintas, and G. Orosz, "Conflict analysis for cooperative maneuvering with status and intent sharing via V2X communication," *IEEE Trans. Intell. Veh.*, early access, doi: 10.1109/TIV.2022.3149796.
- [21] H. M. Wang, S. S. Avedisov, O. Altintas, and G. Orosz, "Multi-vehicle conflict management with status and intent sharing," in *Proc. IEEE Intell. Veh. Symp.*, 2022, pp. 1321–1326.
- [22] *Dedicated Short Range Communications (DSRC) Message Set Dictionary Set*, SAE Int., SAE Standard J2735, 2016.

- [23] *Intelligent Transport Systems (ITS); Vehicular Communications; Basic Set of Applications; Part 2: Specification of Cooperative Awareness Basic Service*, ETSI EN Standard 302 637-2 V1.4.1, 2019.
- [24] L. Zhang and G. Orosz, "Motif-based design for connected vehicle systems in presence of heterogeneous connectivity structures and time delays," *IEEE Trans. Intell. Transp. Syst.*, vol. 17, no. 6, pp. 1638–1651, Jun. 2016.
- [25] W. B. Qin, M. M. Gomez, and G. Orosz, "Stability and frequency response under stochastic communication delays with applications to connected cruise control design," *IEEE Trans. Intell. Transp. Syst.*, vol. 18, no. 2, pp. 388–403, Feb. 2017.
- [26] H. Xing, J. Ploeg, and H. Nijmeijer, "Padé approximation of delays in cooperative acc based on string stability requirements," *IEEE Trans. Intell. Veh.*, vol. 1, no. 3, pp. 277–286, Sep. 2016.
- [27] T. G. Molnár, W. B. Qin, T. Insperger, and G. Orosz, "Application of predictor feedback to compensate time delays in connected cruise control," *IEEE Trans. Intell. Transp. Syst.*, vol. 19, no. 2, pp. 545–559, Feb. 2018.
- [28] C. R. He, J. I. Ge, and G. Orosz, "Fuel efficient connected cruise control for heavy-duty trucks in real traffic," *IEEE Trans. Control Syst. Technol.*, vol. 28, no. 6, pp. 2474–2481, Nov. 2020.
- [29] G. Stépán, *Retarded Dynamical Systems: Stability and Characteristic Functions*. White Plains, NY, USA: Longman Sci. & Tech., 1989.
- [30] M. Krstic, *Delay Compensation for Nonlinear, Adaptive, and PDE Systems*. Berlin, Germany: Springer, 2009.
- [31] N. Kochdumper and M. Althoff, "Sparse polynomial zonotopes: A novel set representation for reachability analysis," *IEEE Trans. Autom. Control*, vol. 66, no. 9, pp. 4043–4058, Sep. 2021.



**Hao M. Wang** received the B.Eng. degree in mechanical and aerospace engineering from Nagoya University, Nagoya, Japan, in 2018. He is currently working toward the Ph.D. degree in mechanical engineering with the University of Michigan, Ann Arbor, MI, USA. His research interests include dynamics and control of connected and automated vehicles.



**Sergei S. Avedisov** (Member, IEEE) received the Ph.D. degree in mechanical engineering from the University of Michigan, Ann Arbor, MI, USA, in 2019. He currently with Toyota R&D InfoTech Labs, Mountain View, CA, USA, as a Cooperative Automated Driving Engineer. His research interests include cooperative automated driving, cooperative perception, cooperative maneuvering, vehicle-to-everything communications, and cooperative platooning in mixed traffic.



**Onur Altintas** (Member, IEEE) received the Ph.D. degree in electronics engineering from The University of Tokyo, Tokyo, Japan. Since 1999, he has been with Toyota Group New Jersey, NJ, USA, Tokyo, Japan, and California, CA, USA, respectively, doing Various Roles. He is currently the InfoTech Labs Fellow and Senior Executive Engineer with Toyota Motor North America R&D, InfoTech Labs, Mountain View, CA, USA. since 2009, he has been the Co-Founder and the General Co-Chair of the IEEE Vehicular Networking Conference. He is also an Associate Editor for IEEE ITS Magazine, IEEE Vehicular Technology Magazine, and IEEE TRANSACTIONS ON INTELLIGENT VEHICLES. He is an IEEE Vehicular Technology Society Distinguished Lecturer.



**Gábor Orosz** (Senior Member, IEEE) received the M.Sc. degree in engineering physics from the Budapest University of Technology, Budapest, Hungary, in 2002 and the Ph.D. degree in engineering mathematics from the University of Bristol, Bristol, U.K., in 2006. He held Postdoctoral Positions with the University of Exeter, Exeter, U.K., and with the University of California, Santa Barbara, CA, USA. In 2010, he joined the University of Michigan, Ann Arbor, MI, USA, where he is currently an Associate Professor of mechanical engineering and of civil and environmental engineering. His research interests include nonlinear dynamics and control, time delay systems, and machine learning with applications to connected and automated vehicles, traffic flow, and biological networks.